PHYSICAL REVIEW B **78**, 035104 (2008)

Fermionic quantum criticality and the fractal nodal surface

Frank Krüger and Jan Zaanen
Instituut-Lorentz, Universiteit Leiden, P.O. Box 9506, 2300 RA Leiden, The Netherlands
(Received 14 April 2008; published 3 July 2008)

The complete lack of theoretical understanding of the quantum critical states found in the heavy-fermion metals and the normal states of the high-T_c superconductors is rooted in a deep fundamental problem of condensed-matter physics: the infamous minus signs associated with Fermi-Dirac statistics render the path integral nonprobabilistic and do not allow the establishment of a connection to critical phenomena in classical systems. Using Ceperley's constrained path-integral formalism, we demonstrate that the workings of scale invariance and Fermi-Dirac statistics can be reconciled. The latter is self-consistently translated into a geometrical constraint structure. We show that this "nodal hypersurface" encodes the scales of the Fermi liquid, and we conjecture that it turns fractal when the system becomes quantum critical. To substantiate this, we analyze the nodal structures of fermionic Feynman backflow wave functions to find that the nodal surface indeed turns into a scale-invariant fractal when the backflow becomes hydrodynamical. Moreover, by following the evaluation of the quasiparticle momentum distribution, we demonstrate that the emergence of scale invariance in the nodal structure is accompanied by a divergence in the effective quasiparticle mass. Such a collapse of a Fermi liquid at a critical point has been observed in the heavy-fermion intermetallics in a spectacular fashion.

DOI: 10.1103/PhysRevB.78.035104 PACS number(s): 71.27.+a, 71.10.Hf, 71.30.+h, 74.72.−h

I. INTRODUCTION

Not long ago, it was taken as physical law that macroscopic systems formed from fermions are Fermi liquids, behaving in a scaling sense as a noninteracting Fermi gas characterized by the Fermi degeneracy scale. This has changed drastically in recent times by the discovery that in some metals the system of electrons behaves very differently. Clear cut examples are the "quantum critical" metallic states found at quantum phase transitions in heavy-fermion compounds;[1–6] there are indications that the metallic states found in the cuprate high-T_c superconductors are of a similar kind.[2,7–14] By tuning a zero-temperature control parameter (such as pressure, magnetic field, and density), one encounters Fermi liquids with different Fermi surfaces, and the quantum critical regime is found at the zero-temperature phase transition, where one metal turns into the other.[5,6] Physical properties in this quantum critical regime are controlled by power laws, indicating that the system has become scale invariant, in analogy to both the thermal phase transitions and the quantum phase transitions in bosonic systems. Albeit rooted in quantum statistics, the Fermi energy is a scale and therefore has to vanish in the quantum critical regime. This is confirmed in a spectacular fashion in the heavy-fermion systems: the mass of the Landau quasiparticles in the Fermi liquids on both sides of the transition should be inversely proportional to the Fermi energy, and this mass is found to diverge to infinity in the quantum critical regime.[5]

How to think about a fermion liquid without Fermi energy? The complete lack of success in understanding the above phenomena is caused by a deep and general methodological problem in many-particle quantum physics.[15] For bosonic problems one can employ the powerful path-integral methods of quantum field theory, directly relating, e.g., the quantum critical state to the well understood statistical physics of classical phase transitions. For fermionic systems this alley is blocked by the infamous minus-sign problem rendering the path integral nonprobabilistic. In fact, the mathematics is as bad as it can be: Troyer and Wiese[16] showed recently that the sign problem falls in the mathematical complexity class "nondeterministic polynomial-time (NP) hard," and the Clay Mathematics Institute has put one of its seven $1 000 000 prizes on the proof that such problems cannot be solved in polynomial time.

Some time ago, Ceperley[17] discovered an alternative representation for the fermionic path integral that does not solve the minus-sign problem in a mathematical sense but has as a virtue that the fermionic statistics is coded in a more manageable way: the "constrained" fermionic path integral. In this framework, the minus signs associated with Fermi-Dirac statistics are self-consistently translated into a geometrical constraint structure (the nodal hypersurface) acting on a residual bosonic dynamics. Although this nodal surface, which contains all the data associated with the differences between bosonic and fermionic matter, is *a priori* not known for an interacting fermion problem, in the scaling limit only its average and global properties should matter. Henceforth, it should be possible in principle to classify all forms of fermionic matter in a phenomenological way by classifying the average geometrical and topological properties of the constraint structure to subsequently use these data as an input to solve the resulting bosonic path-integral problem. This procedure is supposedly a unique extension of the Ginzburg-Landau-Wilson paradigm for bosonic matter to fermionic matter. Employing the Ceperley path integral, in this paper we deliver proof of principle that fermion statistics and emergent scale invariance underlying the critical state can be reconciled.

This paper is organized as follows: In Sec. II we introduce the Ceperley path integral and explain the notion of the "nodal hypersurface." As one anticipates, it has to be that the scales of the Fermi liquid are encoded in the nodal surface

since the residual bosonic dynamics cannot possibly generate these scales by itself. In Sec. III we indeed establish a one-to-one correspondence between the Fermi degeneracy scale and an average nodal pocket dimension, leading to the conjecture that in order for a fermionic system to become critical, the nodal surface has to turn into a scale-invariant fractal. This should be regarded as the most important statement which is substantiated in the remainder of this paper. In Sec. IV we introduce the concept of Feynman and Cohen[18] of incorporating hydrodynamical backflow effects in a quantum mechanical wave function; we show that fermionic backflow wave functions describe many-particle states characterized by a hierarchy of increasing number of particle correlations. The nodal structures of such wave functions are investigated in Sec. V. We find that their nodal surfaces change drastically with increasing backflow strength and turn into a fractal when the backflow becomes hydrodynamical, involving a macroscopic number of particles. A detailed fractal analysis is provided in Sec. VI. In Sec. VII we perform Monte Carlo calculations of the momentum distribution to extract the quasiparticle effective mass as a function of backflow strength. We find that the effective mass diverges exactly at the point where the nodal surface turns into a fractal. Finally, in Sec. VIII our results are summarized and discussed.

II. CONSTRAINED PATH INTEGRAL AND NODAL SURFACE

The fermion sign problem becomes apparent when expressing the many-body density matrix $\rho_F(\mathbf{R},\mathbf{R}';\hbar\beta)$ [with $\mathbf{R}=(\mathbf{r}_1,\ldots,\mathbf{r}_N)$ as the position in dN-dimensional configuration space (d is the spatial dimension and N is the number of particles), and $\beta=1/(k_BT)$ as the inverse temperature] as a path integral over world lines $\{\mathbf{R}_\tau\}$ in imaginary time τ ($0\leq\tau\leq\hbar\beta$), weighted by an action $\mathcal{S}[\mathbf{R}_\tau]$,

$$\rho_F(\mathbf{R},\mathbf{R}';\hbar\beta)=\frac{1}{N!}\sum_{\mathcal{P}}(-1)^p\int_{\mathbf{R}\to\mathcal{P}\mathbf{R}'}\mathcal{D}\mathbf{R}_\tau e^{-\mathcal{S}[\mathbf{R}_\tau]/\hbar},$$

$$\mathcal{S}[\mathbf{R}_\tau]=\int_0^{\hbar\beta}d\tau\left\{\frac{m}{2}\dot{\mathbf{R}}_\tau^2+V(\mathbf{R}_\tau)\right\}, \tag{1}$$

where the sum over all possible $N!$ particle permutations $\mathcal{P}$ accounts for the indistinguishability of the particles and the alternating sign imposes the Fermi-Dirac statistics. Here $p=\mathrm{par}(\mathcal{P})$ denotes the parity of the permutation. Even permutations enter with a positive sign; odd permutations with a negative sign. The term $V(\mathbf{R})$ is a shorthand notation for both external potentials and particle interactions. For simplicity, we have considered spinless fermions. The partition function is obtained as a trace over the diagonal elements of the density matrix, $\mathcal{Z}_N(\beta)=\int d\mathbf{R}\rho_F(\mathbf{R},\mathbf{R};\hbar\beta)$, corresponding to world lines returning to their starting place or a permutation of it. For bosons where the minus signs are absent, the partition function can be viewed as a classical one describing an ensemble of interacting cross-linked ring polymers. However, the fermionic minus signs make this probabilistic interpretation impossible.

Some time ago, Ceperley[17] proved that the fermionic density matrix can be calculated as a path integral analogous to Eq. (1) but summing only over world lines that do not cross the nodes of the density matrix itself, which define for each given initial point $\mathbf{R}_0$ and inverse temperature β a $(dN-1)$-dimensional hypersurface in dN-dimensional configuration space,

$$\Omega_{\mathbf{R}_0,\beta}:=\{\mathbf{R}|\rho_F(\mathbf{R}_0,\mathbf{R};\hbar\beta)=0\}. \tag{2}$$

Those hypersufaces act as infinite potential barriers allowing only node-avoiding world lines $\mathbf{R}_\tau$ with $\rho_F(\mathbf{R},\mathbf{R}_\tau;\tau)\neq 0$ for $0\leq\tau\leq\hbar\beta$.

To calculate the partition function, we have to integrate over the diagonal density matrix $\rho_F(\mathbf{R},\mathbf{R};\hbar\beta)$, which is obtained as a path integral over all world-line configurations $\mathbf{R}\to\mathcal{P}\mathbf{R}$ which do not cross the nodal surface on any time slice and belong to the reach

$$\Gamma_\beta(\mathbf{R})=\{\gamma:\mathbf{R}\to\mathbf{R}'|\rho_F(\mathbf{R},\mathbf{R}(\tau);\tau)\neq 0\}. \tag{3}$$

Because of the antisymmetry of the fermionic density matrix under particle permutations $\mathcal{P}$,

$$\rho_F(\mathbf{R},\mathcal{P}\mathbf{R};\hbar\beta)=\rho_F(\mathcal{P}\mathbf{R},\mathbf{R};\hbar\beta)=(-1)^p\rho_F(\mathbf{R},\mathbf{R};\hbar\beta), \tag{4}$$

all world-line configurations corresponding to odd permutations have to cross a node an odd number of times and are therefore completely removed from the partition function. They are exactly canceled out by all nodes crossing even permutations, and we are left with an ensemble of all node-avoiding world-line configurations corresponding to even permutations,

$$\rho_F(\mathbf{R},\mathbf{R};\hbar\beta)=\frac{1}{N!}\sum_{\mathcal{P},\mathrm{even}}\int_{\gamma:\mathbf{R}\to\mathcal{P}\mathbf{R}}^{\gamma\in\Gamma_\beta(\mathbf{R})}\mathcal{D}\mathbf{R}_\tau e^{-\mathcal{S}[\mathbf{R}]/\hbar}. \tag{5}$$

Remarkably, this representation of an arbitrary fermion problem is not suffering from the "negative probabilities" of the standard formulation. Surely, one cannot negotiate with the NP hardness of the fermion problem and the Ceperley path integral does not solve this problem in the mathematical sense. However, the negative signs are transformed away at the expense of a structure of constraints limiting the Boltzmannian sum over world-line configurations. These constraints in turn can be related to a geometrical manifold embedded in configuration space: the "reach," which is determined by the nodal hypersurfaces of the fermion density matrix. This reach should be computed self-consistently: it is governed by the constrained path integral that itself needs the reach to be computed.

So far, this self-consistent reformulation of the path integral has only been used to study Fermi liquids such as helium-3 (Ref. 19) and many-body hydrogen (Refs. 20 and 21) quantitatively within path-integral Monte Carlo simulations fixing the nodal constraints with a free-particle density matrix. At first glance, this might seem to be a very crude approximation; however, in a scaling sense the Fermi liquid can be viewed as a gas of weakly interacting Landau quasiparticles. As we will see in Sec. III, imposing the nodal constraint structure of noninteracting fermions on the residual bosonic dynamics means nothing but taking Landau's Fermi-liquid paradigm for granted.

Let us further inspect the nodal hypersurface and the workings of the constrained path integral. Since the fermionic density matrix is odd under particle exchanges $\mathcal{P}_{ij}$,

$$\rho_F(\mathbf{R}_0, \mathcal{P}_{ij}\mathbf{R}; \hbar\beta) = -\rho_F(\mathbf{R}_0, \mathbf{R}; \hbar\beta), \tag{6}$$

the density matrix is zero if two fermions are at the same position $\mathbf{r}_i = \mathbf{r}_j$, irrespective of the temperature, the reference point $\mathbf{R}_0$, and the interactions between the particles. Therefore, the Pauli surface

$$P = \bigcup_{i,j}^{i \neq j} \{\mathbf{R} | \mathbf{r}_i = \mathbf{r}_j\} \tag{7}$$

is always a submanifold of the nodal surface $\Omega_{\mathbf{R}_0,\beta}$, whereas the dimensionality of the Pauli surface is dim $P = Nd - d$.

In terms of a complete set of fermionic eigenfunctions $\Psi_\alpha(\mathbf{R})$ with eigenvalues E_α, the fermionic density matrix is given by

$$\rho_F(\mathbf{R}_0, \mathbf{R}; \hbar\beta) = \sum_\alpha e^{-\beta E_\alpha} \Psi_\alpha^*(\mathbf{R}_0) \Psi_\alpha(\mathbf{R}), \tag{8}$$

which, in the case of a nondegenerate ground state $\Psi_0(\mathbf{R})$, converges in the limit $T \to 0$ to $\rho_F(\mathbf{R}_0, \mathbf{R}; \hbar\beta = \infty) = \Psi^*(\mathbf{R}_0)\Psi(\mathbf{R})$. Therefore, the nodal surface $\Omega_{\mathbf{R}_0,\beta}$ of the finite-temperature density matrix becomes independent of the reference point $\mathbf{R}_0$ in the zero-temperature limit and converges to the nodal surface of the ground-state wave function $\Omega := \{\mathbf{R} | \Psi_0(\mathbf{R}) = 0\}$.

In Fig. 1(a) a random cut through the nodal hypersurface of the ground-state wave function $\Psi(\mathbf{r}_1, \ldots, \mathbf{r}_N) = \mathcal{N} \det(e^{i\mathbf{k}_i \mathbf{r}_j})_{i,j=1,\ldots,N}$ of $N = 49$ spinless fermions in a two-dimensional periodic box is shown. This particular particle number corresponds to a set of momenta $\mathbf{k}_1 \ldots, \mathbf{k}_N$ on a grid $\Delta k = 2\pi/L$ (L is the linear dimension of the box) forming a closed shell in momentum space and therefore to a nondegenerate ground state [see inset of Fig. 1(a)]. The cut is obtained by fixing $N-1$ particles at random positions and tracking down the nodes of the wave function, moving the remaining particle over the system. The algorithms used to find the nodes of free fermion and Feynman backflow wave functions studied later on is described in detail in the Appendix. Since the Pauli surface is a lower-dimensional submanifold of the nodal surface, the fixed $N-1$ particles are located on the nodal lines. We find that the nodes are very smooth, forming pockets on the order of the average interparticle spacing r_s. An investigation of the nodal structures of the finite-temperature density matrix[17] shows that this observation holds at any temperature and that the nodal surfaces smoothly approach the ground-state nodes in the limit $T \to 0$.

The workings of the constrained path integral are sketched in Fig. 1. In every time slice τ, one particular particle $\mathbf{r}_1$ sees the nodal constraint structure $\Omega_{\mathbf{R}_0,\beta} := \{\mathbf{R} | \rho(\mathbf{R}_0, \mathbf{R}; \tau) = 0\}$ determined by the positions $\mathbf{r}_2(\tau), \ldots, \mathbf{r}_N(\tau)$ of the $N-1$ other particles on this time slice. Due to the meanderings of the world lines of the $N-1$ particles, the nodal surfaces form a "tent" in space-time attached to the particle world lines since the Pauli surface is always a lower-dimensional nodal hypersurface. Since $\rho_F(\mathbf{R}, \mathbf{R}(\tau); \tau) \neq 0$ for all $0 \leq \tau \leq \hbar\beta$, this nodal tent acts as a hard-core boundary for the world line of the particle $\mathbf{r}_1$ and the particle is not allowed to penetrate or collide with the tent. A world-line configuration, as shown in Fig. 1, does not violate the constraints and contributes to the Ceperley path integral.

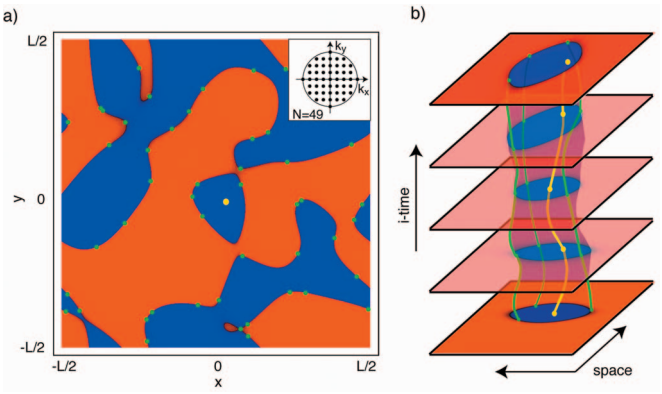

FIG. 1. (Color) (a) Cut through the nodal hypersurface of the ground-state wave function of $N = 49$ free, spinless fermions in a two-dimensional box with periodic boundary conditions. The set of momentum states corresponding to a nondegenerate ground state is shown in the inset. The cut is obtained by fixing $N-1$ fermions at random positions (green dots) and moving the remaining particle (yellow dot) over the system. The nodal-surface cut is given by the interface between red and blue regions, corresponding to negative and positive values of the wave function, respectively, whereas absolute values are encoded in the color shading. The nodal lines connect the $N-1$ fixed particles since the $(Nd-d)$-dimensional Pauli surface is a lower-dimensional submanifold of the $(Nd-1)$-dimensional nodal hypersurface. (b) Sketch of an allowed world-line configuration contributing to the Ceperley path integral. In every time slice τ, one particular particle (yellow dot) sees a nodal surface determined by the positions of the other particles on this time slice. Due to the meanderings of the world lines of the other $N-1$ particles (green), the nodal surfaces form a tent in space-time attached to the particle world lines. This nodal tent acts as a hard-core boundary for the world line of the remaining particle (yellow line).

In a recent tutorial paper,[22] the fermion sign problem has been studied within both the conventional sign-full and the Ceperley path integrals. It turns out that even for the free Fermi gas, for which every student in physics knows the canonical solution, the constrained path integral turns into a highly nontrivial affair. Remarkably, in momentum space the constrained path integral directly leads to a one-to-one correspondence between the Fermi gas and a system of classical atoms forming a Mott insulating state in the presence of a commensurate optical lattice of infinite strength, living in a harmonic potential trap of finite strength.[22] This analogy is literal and the only oddity is that we are talking about an optical lattice system in momentum space. We immediately rediscover our canonical picture of the Fermi gas simply because the dynamics of the world lines becomes trivial due to the conservation of single-particle momentum. However, the workings of the nodal constraints in the real-space formulation remain puzzling to a great extent.[22]

Let us start with the case of free fermions in one space dimension, where the physics of quantum matter can be re-

garded as completely understood.[23] The deep reason is that quantum statistics has no physical meaning in $1+1D$, and it is always possible to find a representation where the sign structure drops out completely. It is instructive to find out how this is processed by the Ceperley path integral. The special status of the one-dimensional case becomes immediately clear since the dimensions of the Pauli surface and the nodal hypersurface coincide and the two manifolds become the same. In this situation it becomes quite easy to read the reach. Start out with a reference point $\mathbf{R}_0=(x_1,x_2,\ldots,x_N)$ ordering the particles, for instance, as $x_1<x_2<\cdots<x_N$. "Spread out" this configuration in terms of world lines meandering along the imaginary time direction and the Pauli-hypersurface reach tells us that the only configurations allowed are those where these world lines never cross each other at any imaginary time. Therefore, the ordering of the particles is preserved at all times and we only have to consider world-line configurations where every particle returns to its starting position. The particles become effectively distinguishable. A more abstract way of saying this is that the Pauli surface (=nodal surface) divides the N-dimensional configuration space into $N!$ disconnected nodal cells, each corresponding to a certain ordering of the particles. We have seen that the Ceperley path integral for the one-dimensional Fermi gas is equivalent to the one for hard-core bosons in $1+1$ dimensions or, from a statistical physics point of view, to the problem of an ensemble of polymers with only steric, hard-core interactions in two dimensions. This "Pokrovsky-Talapov" problem[24] is surely a very serious statistical physics problem since the constraints correspond to infinitely strong delta-function interactions and accordingly everything is about entropic interactions and order-out-of-disorder physics. Remarkably, the one-dimensional fermion story can be completely understood from this radically statistical physics viewpoint[25,26] by using a "self-consistent phonon" method formulated by Helfrich[27] to deal with the entropic interactions associated with biological (extrinsic curvature) membranes.

Obviously, in $d\geq 2$, where the Pauli surface is a lower-dimensional submanifold of the nodal hypersurface, the self-consistency problem inherent to the constrained path integral cannot be resolved like in the one-dimensional case. This is the reason why a general bosonization procedure is lacking in higher dimensions. Although the Ceperley path integral has a much richer structure in higher dimensions, it is surely the case that the higher-dimensional Fermi liquids have to know about the "entropic dynamics" characteristic of the $(1+1)$-dimensional case. However, a generalization of the Helfrich construction to deal with the steric interactions with the nodal tent in a self-consistent way is lacking. Moreover, in contrast to the one-dimensional case, in $d\geq 2$ world-line configurations corresponding to even permutations are *a priori* not ruled out by the constraint structure. Recently, Mitas[28,29] demonstrated that in the case of free spinless fermions, the nodal surface has a minimal tiling property: it divides the configuration space into two nodal cells only. Therefore, it is always possible to find a continuous path $\mathbf{R}\rightarrow\mathcal{P}_{\text{even}}\mathbf{R}$ that does not encounter a node. In other words, all even permutations are on the reach $\Gamma_\beta(\mathbf{R})$ and contribute to the constrained path integral.

Phenomenologically, the Ceperley path integral can be viewed as a bosonic dynamics subject to a geometrical constraint structure and therefore as a statistical physics problem. However, it is a highly nontrivial question as to how to reconstruct the free d-dimensional Fermi gas within this framework using real-space representation (5) and only the one-dimensional case can be regarded as fully understood.[25,26] From the canonical picture we know that the Fermi gas is characterized by a sharp Fermi surface at zero temperature and that the thermodynamics at low temperatures is governed by particle-hole excitations in the vicinity of the Fermi surface, leading, for instance, to a linear specific heat $C(T)\sim k_BT/E_F$ for $T\ll E_F$, irrespective of the spatial dimension. This is surely unconventional for a system of interacting bosons where the spatial dimension enters the exponents of low-temperature expansions in a natural way. Recently, it was conjectured[22] that the nodal surface constraints act in a highly nonlocal way, leading to an effective reduction in the dimensionality in a way that the systems behave qualitatively like soft-core bosons in $1+1D$. Such a "holographic" principle would also explain why the nodal-surface constraints prevent the system from undergoing a Bose condensation at finite temperatures and might relate the emergence of a sharp Fermi surface with a condensation exactly at $T=0$.

III. GEOMETRICAL VIEW ON FERMI-DIRAC STATISTICS AND SCALE INVARIANCE

The constrained path integral is a precise reformulation of the sign-full path integral in terms of an effective bosonic dynamics subject to a geometrical constraint structure and therefore leads the way to a probabilistic, statistical physics interpretation of fermionic systems since the sign structure is absorbed in the nodal hypersurface. A fermionic state such as the Fermi liquid is characterized by scales, the Fermi energy E_F, and the momentum k_F. These scales are alien to any bosonic system. It has to be that these scales are uniquely encoded in the nodal structure, since the residual bosonic system cannot possibly generate these scales by itself.

In Sec. II, we have seen that in dimensions $d\geq 2$ the Pauli surface is a lower-dimensional submanifold of the nodal hypersurface, irrespective of the temperature or the form of interactions. For free fermions we find the nodal surface to smoothly connect the lower-dimensional Pauli surface both at zero temperature [see Fig. 1(a)] and in the finite-temperature case.[17] Therefore, the corresponding nodal structure is characterized by a scale, an average nodal spacing on the order of the average interparticle spacing r_s. This is clearly seen in the two-dimensional nodal surface cut shown in Fig. 1(a): moving one particular particle over the two-dimensional box, we find nodal lines smoothly connecting the $N-1$ other particles, forming pockets with a linear dimension on the order of r_s.

The presence of this scale in the nodal surface can be also deduced by a different argument.[17] From the reduced one-body density matrix, which is simply the Fourier transform of the single-particle momentum distribution $n(\mathbf{r})=\int_{\mathbf{k}}e^{i\mathbf{k}\mathbf{r}}n_{\mathbf{k}}$, given in the limit $T\rightarrow 0$ by

$$n(\mathbf{r}) = \int d\mathbf{R}\Psi^*(\mathbf{r}_1,\mathbf{r}_2,\ldots,\mathbf{r}_N)\Psi(\mathbf{r}_1+\mathbf{r},\mathbf{r}_2,\ldots,\mathbf{r}_N), \quad (9)$$

one obtains an estimate for the nodal spacing. The zeros of $n(r)$ correspond to the average displacement of a particle to be found on a node. For the Fermi gas the momentum distribution in the limit $N\to\infty$ simply turns into a step function, $n_{\mathbf{k}}=\Theta(|\mathbf{k}|-k_F)$, with $\Theta(x)=1$ for $x\leq 0$ and $\Theta(x)=1$ for $x>0$. This leads to the Fourier transform

$$n(\mathbf{r}) = c_d(k_F r)^{-d/2}J_{d/2}(k_F r), \quad (10)$$

where c_d denotes a constant depending on the spatial dimension and $J_{d/2}$ is a Bessel function of the first kind. Asymptotically,

$$n(\mathbf{r}) \sim (k_F r)^{-(d+1)/2}\cos\left(k_F r - \frac{d+1}{4}\pi\right), \quad (11)$$

signaling a long-range periodicity in the nodal structure with an average nodal spacing $r_n \sim k_F^{-1} \sim r_s$. This asymptotic behavior is also generic for the Fermi liquid characterized by a discontinuity in $n(k)$ at the Fermi wave-vector k_F.

From the constrained path integral, a one-to-one correspondence between the existence of a scale in the nodal hypersurface and the Fermi energy E_F can be established by a simple scaling argument. Let us first assume that the nodal hypersurface is characterized by an average nodal pocket dimension on the order of the interparticle spacing r_s characteristic of the Fermi liquid. An allowed world-line configuration is sketched in Fig. 1(b), where we follow the time evolution of the nodal constraint structure seen by one particular particle. In the Ceperley path integral, the world-line configurations $\mathbf{R}_\tau$ are constrained by the reach determined by the condition that the world lines are not allowed to cross the nodal hypersurface of the density matrix itself at any time. From the perspective of one particular particle, this means that the particle has to stay in its nodal pocket at all times $0\leq\tau\leq\hbar\beta$. Due to the meanderings of the world lines of the other particles, the nodal structure seen by the particle fluctuates in time, leading in a time continuum limit to the picture of a nodal surface tent which hangs in space-time and acts as a hard-core boundary for the particle. Since the Pauli surface is at all times a lower-dimensional submanifold of the nodal hypersurface, the world lines of the other particles act as twisted "tent sticks" on which the tent is hanging.

Every particle has to stay within the nodal tent, which is governed by the dynamics of the other particles. At a time scale τ_c, when the average square displacement

$$l^2(\tau) = \langle[\mathbf{r}_i(\tau)-\mathbf{r}_i(0)]^2\rangle = 2d\frac{\hbar}{2m}\tau \quad (12)$$

of the world lines becomes on the order of the average nodal spacing, $l(\tau_c)=r_n$, the particles start to collide with the nodal tent. This leads to the average collision time $\tau_c=(2d)^{-1}(2m/\hbar)r_n^2$, corresponding to an energy scale

$$E_c = \frac{\hbar}{\tau_c} = 2d\frac{\hbar^2}{2m}r_n^{-2} \simeq \frac{2\pi d}{\Gamma^{2/d}\left(\frac{d}{2}+1\right)}\frac{\hbar^2}{2m}n^{2/d}, \quad (13)$$

where in the last step we have assumed that the nodal spacing r_n is on the order of the interparticle spacing r_s, $r_n\simeq r_s$, and introduced the particle density $n=N/V=r_s^{-d}/K_d$, with $K_d=\pi^{d/2}/\Gamma(d/2+1)$ as the volume of the d-dimensional unit sphere. We recognize immediately that Eq. (13) is just the expression for the Fermi energy in d dimensions, $E_F\simeq E_c$. In the case of free fermions, we can even be more quantitative and estimate the average nodal pocket dimension r_n as the first zero of the reduced one-body density matrix $n(r)$ [Eq. (10)], which in d dimensions is given by $r_n=z_d/k_F$, with z_d as the first zero of the Bessel function $J_{d/2}(z)$. This yields $E_c=\alpha_d E_F$, with $\alpha_2\approx 0.27$ and $\alpha_3\approx 0.30$ in two and three dimensions, respectively.

From the above scaling argument, we have learned that an average nodal pocket dimension is dynamically related to a typical time scale τ_c on which the particles feel the steric constraints imposed by the nodal-surface tent. The Fermi energy we rediscover immediately as the corresponding energy scale $E_F=\hbar/\tau_c$. What does this imply for a critical fermionic state having no knowledge whatsoever about E_F as required by the underlying scale invariance and as observed in various experiments? Turning the above scaling argument around, the absence of a Fermi degeneracy scale immediately implies that the nodal surface cannot possibly carry a characteristic scale. The nodal-surface constraints have to act in the same way on all time and length scales and therefore, the nodal surface of any fermionic critical state has to be a scale-invariant fractal. Hence, by using scaling arguments resting on the constrained path integral, we have discovered a phenomenological principle: The *collapse* of the Fermi liquid at a *quantum critical point* as observed experimentally, for instance, in the heavy-fermion metals is necessarily associated with a *qualitative change* in the nodal surface *from a smooth to a fractal geometry*. This should be regarded as the most important finding reported in this paper since it identifies the probabilistic constrained path integral as the mathematical framework in which to reconcile the workings of Fermi-Dirac statistics and scale invariance.

IV. FEYNMAN BACKFLOW WAVE FUNCTIONS: PRELIMENARIES

In Sec. III we have convinced ourselves that a critical fermionic state is necessarily characterized by an underlying fractal nodal surface. However, an inherent difficulty of the present approach is that in order to study nodal structures associated with nonconventional states, a wave-function ansatz is required.

Let us focus on a concept introduced by Feynman and Cohen[18] incorporating hydrodynamical backflow effects in a quantum mechanical wave-function. They argued that the roton in ^{4}He is like a single mobile atom which is, however, dressed up by collective motions in the liquid. Helium is a nearly incompressible fluid in the hydrodynamical sense, and the density in the neighborhood of the moving particle should be barely altered. As a consequence, there has to be a

backflow of other particles conserving the total current and leading to an enhancement of the effective mass of this quasiparticle, which can be described quantum mechanically by taking a plane-wave function $\exp(i\mathbf{k}\tilde{\mathbf{r}}_i)$ with a collective quasiparticle coordinate

$$\tilde{\mathbf{r}}_i = \mathbf{r}_i + \sum_{j(\neq i)} \eta(r_{ij})(\mathbf{r}_i - \mathbf{r}_j), \tag{14}$$

where $\mathbf{r}_i$ are the coordinates of the bare particles, $r_{ij} = |\mathbf{r}_i - \mathbf{r}_j|$, and $\eta(r)$ is a smoothly varying function falling off like $\sim r^{-3}$ on large distances corresponding to hydrodynamical, dipolar backflow of an incompressible fluid in two dimensions. Much later, it was found out that by using fermionic backflow wave functions of the form $\Psi \simeq \det(e^{i\mathbf{k}_i\tilde{\mathbf{r}}_j})$ for node fixing, one obtains excellent variational energies for the fermionic ^{3}He quantum fluid[30] and the homogeneous electron gas.[31,32]

It easy to check that such Slater determinants of plane-wave functions of collective backflow coordinates indeed obey Fermi-Dirac statistics since the permutation of two particles $\mathbf{r}_i$ and $\mathbf{r}_j$ leads to an interchange of the collective coordinates $\tilde{\mathbf{r}}_i$ and $\tilde{\mathbf{r}}_j$ without changing the other collective coordinates and therefore to an overall sign change of the determinant. Therefore, as for any fermionic state the lower-dimensional Pauli surface is still a submanifold of the nodal hypersurface of fermionic backflow wave functions. However, due to the collectiveness built into these wave functions, one might expect the nodal hypersurfaces to be radically different from the smooth free fermion case. This is supported by an earlier work[33] that reported a precursor of the roughening of the nodal structure in the regime of weak backflow.

We would like to emphasize that the hydrodynamical Feynman backflow built into the fermionic wave functions has nothing to do with the conventional notion of backflow in a Fermi liquid since it involves interactions between a macroscopic number of particles at the same time. To rationalize this, we will derive an expansion of the Hamiltonian of which the backflow wave functions are eigenstates. In terms of collective backflow coordinates (14), we are simply dealing with a gas of free quasiparticles and the exact Hamiltonian of the system is therefore given by

$$\hat{\mathcal{H}} = \sum_{\mathbf{k}} \epsilon_{\mathbf{k}} \tilde{c}^\dagger_{\mathbf{k}} \tilde{c}_{\mathbf{k}}, \tag{15}$$

where we have introduced the operators $\tilde{c}^\dagger_{\mathbf{k}}$ and $\tilde{c}_{\mathbf{k}}$, creating and annihilating a backflow particle with momentum $\mathbf{k}$, respectively. To find the representation of this Hamiltonian in terms of the bare-particle operators $c^\dagger_{\mathbf{k}}$ and $c_{\mathbf{k}}$, let us first derive an expansion of the N-particle backflow wave function in terms of free-particle states. Using the above Fermi operators for backflow and bare particles, a general relation can be written as

$$\begin{aligned} |\mathbf{k}_1, \ldots, \mathbf{k}_N\rangle_{\mathrm{bf}} &= \tilde{c}^\dagger_{\mathbf{k}_1} \cdots \tilde{c}^\dagger_{\mathbf{k}_N} |0\rangle \\ &= \int_{\mathbf{q}_1,\ldots,\mathbf{q}_N} \Gamma_{\mathbf{q}_1,\ldots,\mathbf{q}_N} c^\dagger_{\mathbf{k}_1+\mathbf{q}_1} \cdots c^\dagger_{\mathbf{k}_N+\mathbf{q}_N} |0\rangle \\ &= \int_{\mathbf{q}_1,\ldots,\mathbf{q}_N} \Gamma_{\mathbf{q}_1,\ldots,\mathbf{q}_N} \times |\mathbf{k}_1+\mathbf{q}_1, \ldots, \mathbf{k}_N+\mathbf{q}_N\rangle, \end{aligned} \tag{16}$$

where the function Γ is defined as the Fourier transform

$$\Gamma_{\mathbf{q}_1,\ldots,\mathbf{q}_N} = \frac{1}{V^N} \int d^d\mathbf{r}_1 \cdots d^d\mathbf{r}_N \times \prod_i e^{-i\mathbf{q}_i\mathbf{r}_i} \exp \sum\nolimits_{j(\neq i)} f_i(\mathbf{r}_{ij}), \tag{17}$$

and for abbreviation we have defined $f_i(\mathbf{r}_{ij}) = i\eta(r_{ij})\mathbf{k}_i(\mathbf{r}_i - \mathbf{r}_j)$. General expressions (16) and (17) can be further evaluated by expanding the exponentials,

$$\begin{aligned} \prod_i \exp \sum\nolimits_{j(\neq i)} f_i(\mathbf{r}_{ij}) &= 1 + \sum_{i,j}^{i\neq j} f_i(\mathbf{r}_{ij}) \\ &\quad + \frac{1}{2} \sum_{i,j,m,n}^{i\neq j, m\neq n} f_i(\mathbf{r}_{ij}) f_m(\mathbf{r}_{mn}) + \cdots, \end{aligned} \tag{18}$$

which leads to an expansion of the operator $\hat{A}$, which transforms the free fermion state to the backflow state,

$$|\mathbf{k}_1, \ldots, \mathbf{k}_N\rangle_{\mathrm{bf}} = \hat{A} |\mathbf{k}_1, \ldots, \mathbf{k}_N\rangle. \tag{19}$$

Up to second order in the backflow function $\eta(r)$, we obtain

$$\begin{aligned} \hat{A}_0 &= 1, \\ \hat{A}_1 &= \sum_{i,j}^{i\neq j} \int_{\mathbf{q}} \tilde{f}_i(\mathbf{q}) c^\dagger_{\mathbf{k}_i+\mathbf{q}/2} c_{\mathbf{k}_i} c^\dagger r_{\mathbf{k}_j-\mathbf{q}/2} c_{\mathbf{k}_j}, \\ \hat{A}_2 &= \frac{1}{2}\hat{A}_1^2 = \frac{1}{2} \sum_{i,j,m,n}^{i\neq j, m\neq n} \int_{\mathbf{q}} \int_{\mathbf{q}'} \tilde{f}_i(\mathbf{q}) \tilde{f}_m(\mathbf{q}') c^\dagger_{\mathbf{k}_i+\mathbf{q}/2} c_{\mathbf{k}_i} \\ &\quad \times c^\dagger_{\mathbf{k}_j-\mathbf{q}/2} c_{\mathbf{k}_j} c^\dagger_{\mathbf{k}_m+\mathbf{q}'/2} c_{\mathbf{k}_m} c^\dagger_{\mathbf{k}_n-\mathbf{q}'/2} c_{\mathbf{k}_n}, \end{aligned} \tag{20}$$

where we have introduced the Fourier transform

$$\tilde{f}_i(\mathbf{q}) = \frac{1}{V} \int d^d\mathbf{r} e^{-i\mathbf{q}\mathbf{r}} f_i(\mathbf{r}). \tag{21}$$

The Hamiltonian transforms under the inverse of the operator $\hat{A}$, namely,

$$\hat{\mathcal{H}} = (\hat{A}^\dagger)^{-1} \hat{\mathcal{H}}_0 \hat{A}^{-1}, \tag{22}$$

where $\hat{\mathcal{H}}_0 = \Sigma_{\mathbf{k}} \epsilon_{\mathbf{k}} c^\dagger_{\mathbf{k}} c_{\mathbf{k}}$ is the Hamiltonian for the noninteracting Fermi gas. To zeroth order (no backflow), we trivially obtain $\hat{A} = 1$ and therefore $\hat{\mathcal{H}} = \hat{\mathcal{H}}_0$. The next corrections to the Hamiltonian in first and second orders of the backflow function $\eta(r)$ are given by

$$\hat{\mathcal{H}}_1 = -\hat{A}_1^\dagger \hat{\mathcal{H}}_0 - \hat{\mathcal{H}}_0 \hat{A}_1,$$

$$\hat{\mathcal{H}}_2 = \hat{A}_1^\dagger \hat{\mathcal{H}}_0 \hat{A}_1 + \frac{1}{2}(\hat{A}_1^\dagger)^2 \hat{\mathcal{H}}_0 + \frac{1}{2}\hat{\mathcal{H}}_0 \hat{A}_1^2. \tag{23}$$

From the above expansion, it becomes immediately clear that Feynman backflow generates a hierarchy of processes involving an increasing number of particles. To zeroth order in η, the backflow state is, of course, trivially identical to the free fermion one, $\hat{A}_0=1$. Whereas the first-order terms $\hat{A}_1$ correspond solely to pair scattering processes to second-order $\hat{A}_2$, the Hamiltonian already contains three- and four-body interactions. The expansion in powers of $\eta(r)$ is under control only if the strength of the backflow is sufficiently weak. In this case the backflow can be to a good approximation rationalized in terms of two-body interactions. However, when the backflow becomes strong, the expansion breaks down and n-body interactions of arbitrary order are no longer negligible. Surely, such a state characterized by hydrodynamical backflow in a true sense involving a macroscopic number of particles cannot be obtained perturbatively since it requires an infinite number of vertex corrections.

Anticipating that we will find a critical non-Fermi-liquid state when the backflow turns hydrodynamical, it might well be that this gives way to general wisdom. The Fermi liquid is known to be remarkably stable as long as one is dealing with a scaling limit where two-(quasi)particle interactions are less irrelevant than the three-particle interactions and so forth. The backflow ansatz seems to suggest that it is a necessary condition for the destruction of the Fermi liquid that the scaling flow is such that n-point interactions, with n arbitrarily large, are equally marginal.

V. NODAL STRUCTURE OF BACKFLOW WAVE FUNCTIONS

Let us now proceed to calculate the nodal surfaces of fermionic Feynman backflow wave functions. In particular, we take

$$\Psi(\mathbf{r}_1, \ldots, \mathbf{r}_N) = \mathcal{N} \det(e^{i\mathbf{k}_i \tilde{\mathbf{r}}_j})_{i,j=1,\ldots,N}, \tag{24}$$

with a set $\mathbf{k}_1 \ldots, \mathbf{k}_N$ of momenta corresponding to a nondegenerate ground state in the free case [see Fig. 1(a)], and use collective backflow coordinates (14) with a backflow function

$$\eta(r) = \frac{a^3}{r^3 + r_0^3}, \tag{25}$$

having the characteristic r^{-3} tail of hydrodynamical dipolar backflow in a two-dimensional incompressible fluid. Further, we have introduced a small-distance cutoff r_0 and a length a to make the backflow function $\eta(r)$ dimensionless and to control the strength of the backflow. The expansion in terms of the backflow strength should be controlled by the dimensionless parameter $\alpha=a/r_s$, with r_s as the average interparticle spacing. However, on the wave-function level, there is no restriction to small values of α and we can in principle follow the evaluation of the nodal surface into a regime where the expansion breaks down and backflow is governed by infinite number of particle correlations.

Like in the free fermion case, we calculate the nodal structure on two-dimensional cuts obtained by fixing $N-1$ particles at random positions and searching for nodes when moving the remaining particle over the box. Due to the collectiveness of the backflow wave functions, the complexity of the problem increases significantly compared to the free case since the change in the coordinate of one particular particle leads to a change in all collective coordinates $\{\tilde{\mathbf{r}}_i\}$ and we have to recalculate the full $N \times N$ determinant for every point on the cut. For details on the node-searching algorithm, we refer the reader to the Appendix.

In Fig. 2 the evaluation of the nodal surface on a particular cut for $N=49$ particles with increasing backflow strength $\alpha=a/r_s$ is shown. As a reference, in the upper left frame the nodal-surface cut for free fermions corresponding to $\alpha=0$ is plotted. As discussed earlier the nodal surface smoothly connects the lower-dimensional Pauli surface, forming pockets with a characteristic dimension on the order of the interparticle spacing r_s. For small values of α, additional nodal pockets start to develop for small particle separations (in the vicinity of the Pauli surface), consistent with the local roughening of the nodal surface reported previously,[33] whereas on larger scales the nodal structure looks similar to that in the free case. The size of these clouds of additional nodal pockets is much smaller than the interparticle spacing, suggesting that backflow is basically governed by two-particle correlations, as also expected from the expansion in terms of powers of $\eta(r)$ [see Eq. (16)]. This is confirmed by the analysis of the nodal structure of two particles subject to a mutual backflow. For small particle separations, we basically observe the same local change in the nodal surface as in the N-particle case. These local two-particle effects have surely nothing to do with the concept of collective hydrodynamical backflow as originally introduced by Feynman.[18] Moreover, a decrease in the small-distance cutoff r_0 leads to the development of a local unphysical fractality in the clouds completely unrelated to collective behavior. A closer inspection of the fermionic backflow wave functions used for node fixing in Monte Carlo calculations shows that they belong to the regime of weak backflow accounting for local two-particle correlations ("exchange-correlation hole") in a crude way. This is further amplified by the fact that even short-range backflow functions $\eta(r)$ have been commonly used.[34]

We find that the size of the clouds of additional nodal pockets scale linearly with α, identifying the parameter a as the effective backflow range (see Fig. 2). With increasing α, the clouds start to overlap more and more, forming clusters of interfering backflow patterns signaling that the nodal structure can no longer be understood in terms of two-particle correlations and that the backflow becomes more and more collective. The nodal surface seems to develop a scale invariance up to this cluster size ξ, which can be further amplified by decreasing the small-distance cutoff r_0. At the point where α becomes on the order of unity, the backflow becomes collective, involving a macroscopic number of particles. At this point, ξ becomes on the order of the system size and the nodal surface seems to turn into a fractal.

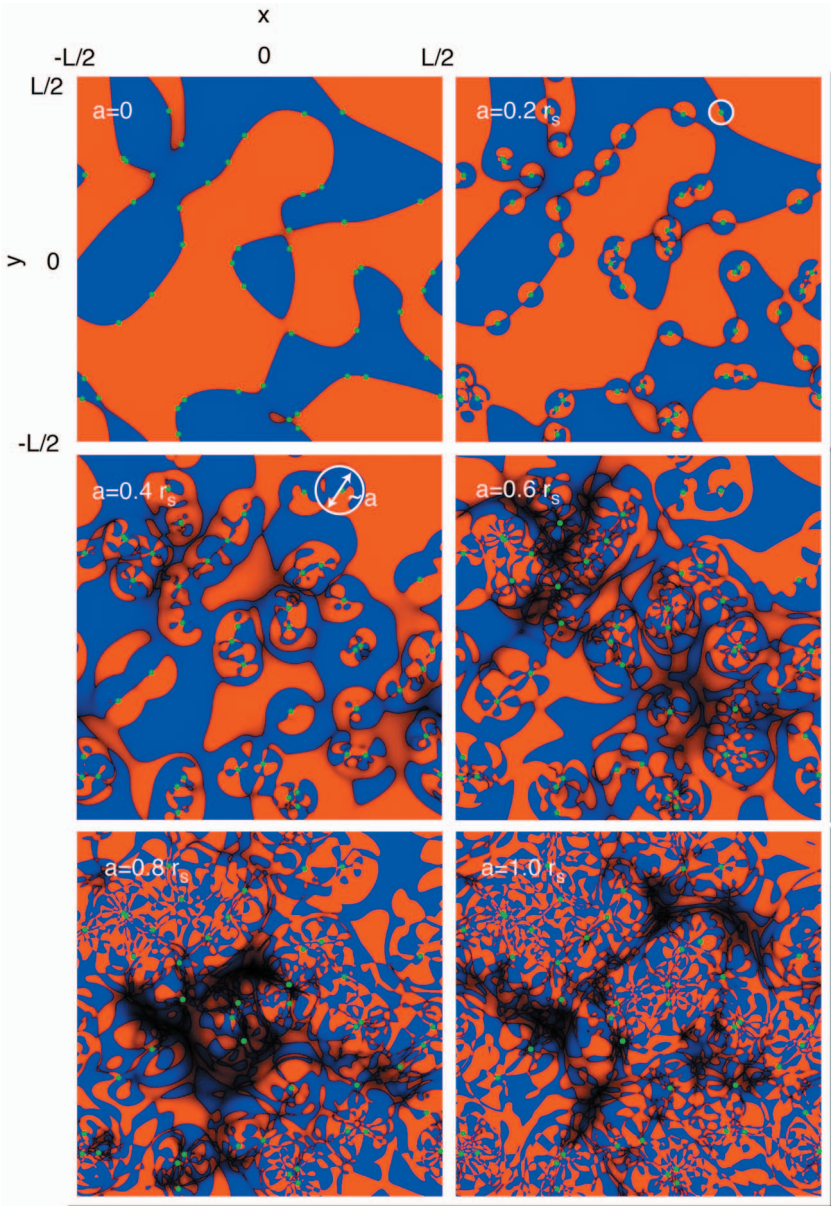

FIG. 2. (Color) Two-dimensional cuts through the nodal hypersurfaces of fermionic backflow wave functions for $N=49$ particles and different values of the backflow strength $\alpha=a/r_s$ and a small-distance cutoff $r_0/r_s=0.1$. The cuts are obtained in the same way as described in the caption of Fig. 1. For $\alpha=0$ we recover the smooth nodal structure of free fermions. With increasing backflow strength, additional clouds of nodal pockets start to develop. The linear dimension of these clouds scales linearly with α. When the effective backflow range a becomes on the order of the interparticle spacing r_s, the nodal surface qualitatively changes its geometry and seems to turn into a fractal.

VI. FRACTAL ANALYSIS

To demonstrate that we indeed succeeded to produce a scale-invariant nodal surface, we evaluate the correlation integral $C(r)$, which counts the number of pairs of points $\{\mathbf{X}_i\}$ on the nodal surface with a separation smaller than r,

$$C(r) = \lim_{x\to\infty} \frac{1}{n(n-1)} \sum_{i,j=1,\ldots,n}^{i\neq j} \Theta(|\mathbf{X}_i - \mathbf{X}_j| - r), \qquad (26)$$

where $\Theta(x)$ denotes the Heaviside function; $\Theta(x)=1$ for $x \leq 0$ and $\Theta(x)=1$ for $x>0$. For a fractal object the correlation integral, which is simply the integral of the point-to-point correlation function, is expected to scale as a power law, $C(r) \sim r^{D_H}$, with the exponent D_H very close to the Hausdorff dimension of the fractal.[35]

Of course, it is impossible to map out the full high-dimensional nodal surface. Therefore we instead perform the fractal analysis on various two-dimensional random cuts as shown in Fig. 2. Whereas for these cut pictures we have calculated, solely for illustrational purposes, we need the values of the wave function on all points of a fine two-dimensional grid; for the fractal analysis we need only the points on the nodes which in Fig. 2 correspond to the interface between positive and negative regions. To track down the nodes on the cut, we use a triangulation method directly following the nodal lines. This algorithm, which is described in detail in the Appendix, has the virtue of omitting the calculation of the highly collective wave functions on too many points away from the nodes. To test the algorithm, we have calculated the nodes on the same two-dimensional cut and for the same parameters as in Fig. 2 and found perfect agreement between the nodal points obtained from the triangulation method (see insets of Fig. 3) and the interfaces in Fig. 2.

A fractal nodal surface in full dN-dimensional configuration space must have a Hausdorff dimension D_H between $dN-1$, which is the dimension of a regular nodal hypersurface, and dN, the dimension of the embedding configuration

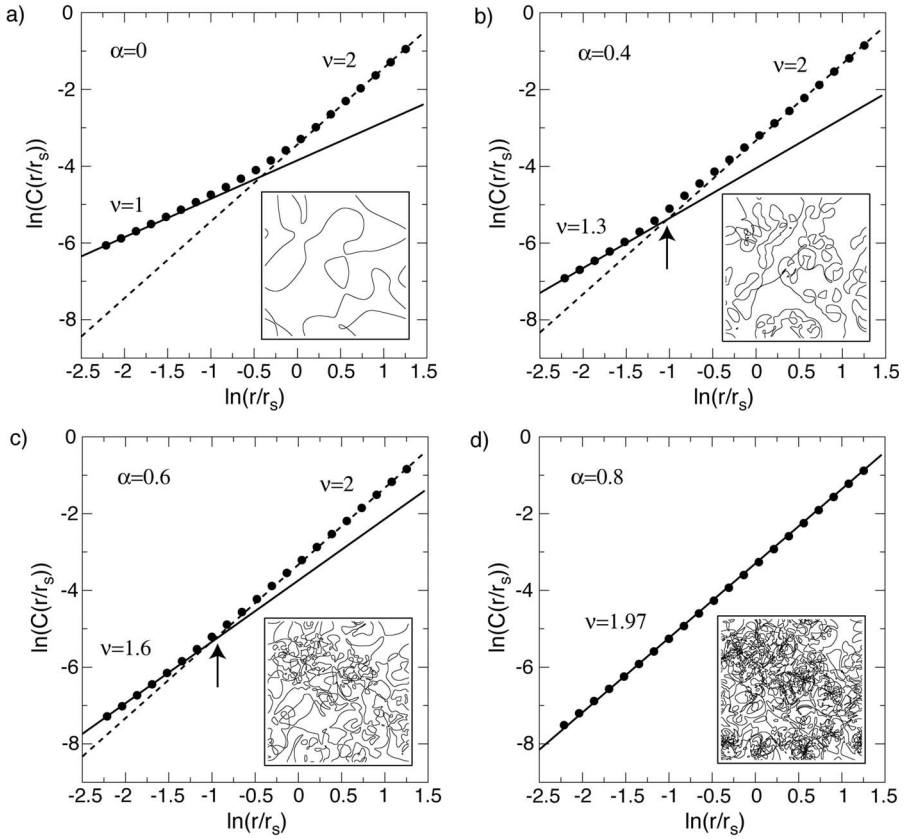

FIG. 3. Correlation integrals $C(r)$ as a function of separation in a log-log plot for the same nodal-surface cuts and backflow strengths α as used in Fig. 2. The corresponding nodal-surface cuts are shown in the insets. The nodal surface turns into a fractal at a critical backflow strength $\alpha_c \approx 0.8$.

space. Therefore, in $d=2$ space dimensions, one expects on a two-dimensional cut a fractal dimension $\nu=D_H/N$ in the range $2-1/N<\nu<2$. Hence, with increasing number of particles N, we expect the Hausdorff dimension ν of the nodal-surface cut to increase and to approach $\nu=2$ in the limit $N\rightarrow\infty$. This means that for a large number of particles, the nodes on the cuts should be very close to space filling. Notice that the visual inspection of the cuts can be quite misleading regarding the space-filling properties of the high-dimensional nodal surface.

Let us first analyze correlation integrals (26) for the nodal-surface cuts shown in Fig. 2. To correct for finite-size effects, we multiply $C(r)$ by a function, $g(r/L)$, which normalizes the correlation integral by the number of available pairs of separation smaller than r in a finite box $[-L/2,L/2]\times[-L/2,L/2]$. This function is given by $g(r/L)=\pi r^2/\langle A_r(x,y)\rangle_{L^2}$, where $A_r(x,y)$ denotes the part of the area of a circle with midpoint (x,y) and radius r lying within the box. The average $\langle\cdots\rangle_{L^2}$ has to be taken over all points (x,y) in the box. A straightforward calculation yields for $r\leq L/2$

$$g\left(\frac{r}{L}\right)=\left[\left(1-\frac{8}{3\pi}\left(\frac{r}{L}\right)+\left(\frac{11}{3\pi}-1\right)\left(\frac{r}{L}\right)^2\right]^{-1}. \quad (27)$$

The evolution of the correlation integral is shown in Fig. 3. Without backflow ($\alpha=0$), where the nodes on the two-dimensional cut are smooth lines with an average spacing on the order of the interparticle distance r_s, we find $\nu=1$ for small distances, as expected for a one-dimensional object, and a crossover around r_s to an exponent $\nu=2$ on larger scales [Fig. 3(a)]. This crossover signals the existence of an average nodal pocket dimension $\sim r_s$: On this scale nodal lines start to see each other, forming an object which looks two dimensional on larger scales. For small backflow strength α, we introduce another scale $a=\alpha r_s$ in the system which we have identified with the size of additional clouds of nodal pockets. The change in the small-distance behavior can clearly be seen in the correlation integral, where we find fractality with a nonuniversal dimension ν up to the scale a. On smaller scales, this fractality is cut off by the parameter $r_0\ll r_s$. At the larger scale r_s, we again find a crossover to $\nu=2$, signaling the existence of an average nodal pocket dimension comparable to the free case [see Fig. 3(b)]. Increasing α further, both the range of the scale-invariant behavior and the fractal dimension increase [Fig. 3(c)].

At a critical value $\alpha_c\approx 0.8$, where a becomes comparable to r_s, both scales suddenly disappear and the correlation integral $C(r)$ turns into a power law up to the system size, demonstrating that the nodal-surface cut has become a scale-invariant fractal with a Hausdorff dimension $\nu\approx 1.97$ very close to the space-filling dimension $d=2$ [see Fig. 3(d)]. For values of $\alpha\geq\alpha_c$ the nodal structure remains fractal without further increase in the Hausdorff dimension ν.

We have found that with increasing backflow strength α, the backflow clouds start to interfere, forming clusters of linear dimension ξ (see Fig. 2). This length scale should be identified with the correlation length of scale-invariant fluctuations corresponding to the crossover in $C(r)$ from scale-invariant to regular behavior on larger scales as indicated by arrows in Figs. 3(b) and 3(c). Approaching the critical value α_c, ξ rapidly becomes on the order of the system size and

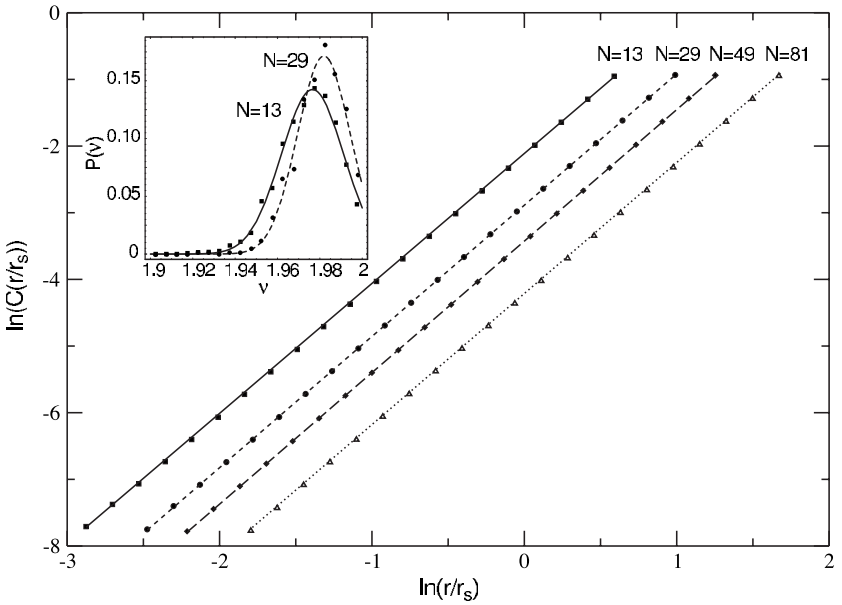

FIG. 4. Correlation integrals $C(r)$ for random two-dimensional nodal-surface cuts for different numbers of particles and a critical backflow strength $\alpha_c=0.8$. In all cases we find scale-invariant behavior and Hausdorff dimensions slightly below 2. In the inset we plotted the distributions $P(\nu)$ of the Hausdorff dimensions obtained from a large number of random two-dimensional cuts for $N=13$ and $N=29$ particles.

should diverge in the limit $N\to\infty$. However, it is not possible to track down the divergence of the correlation length quantitatively since we cannot follow the crossover in a regime sufficiently close to α_c.

In Fig. 4 we have plotted the correlation integrals $C(r)$ for different numbers of particles at a fixed density $n=N/V \sim r_s^{-2}$, taking the critical backflow strength $\alpha_c=0.8$. We find a power-law behavior over approximately three decades for the biggest system and exponents ν slightly below 2 in all cases. Further, we observe a small increase in the fractal dimension consistent with the inequality $2-1/N<\nu<2$. For smaller systems it is possible to calculate $C(r)$ for a large number of random two-dimensional cuts. The resulting distributions $P(\nu)$ of the Hausdorff dimensions are shown in the inset of Fig. 4 for $N=13$ and $N=29$ particles. For the larger number of particles, the Gaussian distribution becomes narrower and shifts toward $\nu=2$. From the mean $\bar{\nu}$ and the width of the distribution $P_N(\nu)$, we estimate for the Hausdorff dimension of the nodal surface in full dN-dimensional configuration space $D_H=N\bar{\nu}=2N-1+R_H$, with $R_H=0.6\pm0.3$ and $R_H=0.5\pm0.3$ for $N=13$ and $N=29$, respectively.

VII. MOMENTUM DISTRIBUTION AND EFFECTIVE-MASS DIVERGENCE

We have demonstrated that fermionic Feynman backflow wave functions exhibit very rich nodal structures and that by increasing the backflow strength α, it is possible to continuously tune the nodal surface from the smooth one of the free gas to a scale-invariant fractal. On the other hand, we showed that the Fermi degeneracy scale has a simple geometrical meaning: it has a one-to-one correspondence to an average nodal pocket dimension. This scale disappears as we approach the critical backflow strength. Therefore, we succeeded to produce a critical fermionic state of matter lacking a Fermi degeneracy scale.

Experimentally, the collapse of a Fermi-liquid state toward a quantum critical point has been observed in a spectacular fashion in the heavy-fermion metals. From Hall resistivity measurements,[6] it has been concluded that the Fermi surface undergoes a discontinuous jump at the quantum critical point, signaling that there is no sense of a Fermi surface underlying the critical state. How does the system get rid of the Fermi energy scale? The quasiparticles in the Fermi liquids on both sides of the transition are characterized by an effective mass $m^*\sim 1/E_F$, which diverges as a power law as one approaches the critical point as, for example, clearly seen in measurements of the linear specific heat coefficient $C(T)/T\sim m^*$.[5] A theoretical understanding of how the quasiparticles get heavier and heavier and finally completely die is completely lacking, and the question remains as to what extent collective backflow wave functions can account for such a mysterious behavior.

The quasiparticle effective mass m^* is per definition given by

$$\frac{m^*}{m}=\left.\frac{m}{k}\frac{d}{dk}\epsilon(\mathbf{k})\right|_{k=k_F}, \tag{28}$$

where m is the bare electron mass and can be expressed by use of the Dyson equation[36,37] in terms of the real part of the quasiparticle self-energy $\Sigma(\mathbf{k},\omega)$ as

$$\frac{m^*}{m}=\left.\frac{1-\frac{\partial}{\partial\omega}\mathrm{Re}\,\Sigma(\mathbf{k},\omega)}{1+\frac{m}{k}\frac{\partial}{\partial k}\mathrm{Re}\,\Sigma(\mathbf{k},\omega)}\right|_{k=k_F,\omega=0}. \tag{29}$$

Under the conventional assumption that the momentum dependence of the real part of the self-energy remains nonsingular, a divergence in the quasiparticle mass m^* can be directly related to a vanishing quasiparticle pole strength

$$Z=\left.\left(1-\frac{\partial}{\partial\omega}\mathrm{Re}\,\Sigma(\mathbf{k},\omega)\right)^{-1}\right|_{k=k_F,\omega=0}, \tag{30}$$

which defines the size of the effective Fermi-surface discontinuity; the disappearance of the discontinuity Z in the qua-

siparticle momentum distribution $n(\mathbf{k})$ would correspond to an effective-mass divergence $m^*/m \sim 1/Z$.

Since Z can be derived from the $n(\mathbf{k})$ jump, we calculate the single-particle momentum distribution of backflow wave functions to establish a connection between an effective-mass divergence and the disappearance of a scale in the nodal hypersurface. From the ground-state wave function, the single-particle momentum distribution at zero temperature can be calculated as a Fourier transform of reduced one-body density matrix (9),

$$n(\mathbf{k}) = (2\pi)^{-2} \int d\mathbf{r} \int d\, \mathrm{Re}^{i\mathbf{k}\mathbf{r}} \Psi^*(\mathbf{r}_1, \mathbf{r}_2, \ldots, \mathbf{r}_N) \times \Psi(\mathbf{r}_1 + \mathbf{r}, \mathbf{r}_2, \ldots, \mathbf{r}_N). \quad (31)$$

For the backflow wave functions, this high-dimensional integral cannot be calculated analytically since the bare coordinates enter via the transformations to collective coordinates (14) in a highly nontrivial way and an expansion in terms of the backflow strength α [Eq. (16)] breaks down as we approach the critical value, where the backflow becomes highly collective, involving a macroscopic number of particles at the same time. Of course, numerically such integrals in $D = dN + d$ dimensions can be calculated only by means of Monte Carlo integration. The basic idea is very simple and is based on the central limit theorem. Let $\{\mathbf{x}_1, \ldots, \mathbf{x}_n\}$ be a set of uncorrelated points in a very-high-dimensional space which are distributed according to a probability distribution $P(\mathbf{x})$ fulfilling the requirements $P(\mathbf{x}) \geq 0$ and $\int d\mathbf{x} P(\mathbf{x}) = 1$. Let us introduce a new random variable $Y_f = [f(\mathbf{x}_1) + \cdots + f(\mathbf{x}_n)]/n$, where f is some arbitrary real-valued function with mean μ_f and variance σ_f^2 given by

$$\mu_f = \langle f(\mathbf{x}) \rangle_P = \int d\mathbf{x} f(\mathbf{x}) P(\mathbf{x}), \quad (32)$$

$$\sigma_f^2 = \langle [f(\mathbf{x}) - \langle f(\mathbf{x}) \rangle]^2 \rangle_P = \int d\mathbf{x} [f(\mathbf{x}) - \mu_f]^2 P(\mathbf{x}). \quad (33)$$

Then it can be shown that under rather general conditions[38] that the central limit theorem applies and that for large enough n the variable Y_f is normally distributed with mean μ_f and standard deviation $\sigma_f/\sqrt{n}$, irrespective of the dimension. These ideas can easily be applied to high-dimensional integrals such as for the momentum distribution we want to calculate. To establish a connection to Eq. (33), we simply rewrite the integral by introducing a probability distribution, $I = \int d\mathbf{x} g(\mathbf{x}) = \int d\mathbf{x} f(\mathbf{x}) P(\mathbf{x})$, with $f(\mathbf{x}) = g(\mathbf{x})/P(\mathbf{x})$. The integral I can then be estimated by sampling a large number n of points x_i according to the probability distribution $P(\mathbf{x})$ as

$$I = \int d\mathbf{x} g(\mathbf{x}) = \left\langle \frac{g(\mathbf{x})}{P(\mathbf{x})} \right\rangle_P \approx \frac{1}{n} \sum_{i=1}^{n} \frac{g(\mathbf{x}_i)}{P(\mathbf{x}_i)}, \quad (34)$$

whereas the variance of the estimate of the integral is given by

$$\frac{\sigma_f^2}{n} \approx \frac{1}{n^2} \sum_{i=1}^{n} \left[\frac{g(\mathbf{x}_i)}{P(\mathbf{x}_i)} - \frac{1}{n} \sum_{j=1}^{n} \frac{g(\mathbf{x}_j)}{P(\mathbf{x}_j)} \right]^2, \quad (35)$$

from which we obtain $\pm \sigma_f/\sqrt{n}$ as an estimate of the size of the error bar on the computed value of I. Obviously, for a given sample size, the variance depends significantly on the choice of the probability function $P(\mathbf{x})$. In the case of the integral $n(\mathbf{k})$ [Eq. (31)], we have tried different distributions and found the best convergence for the choice

$$P(\mathbf{x}) = P(\mathbf{R}, \mathbf{r}) = |\Psi(\mathbf{R})|^2, \quad (36)$$

giving for every $\mathbf{k}$ point the value of $n(\mathbf{k})$ as the sample average

$$n(\mathbf{k}) = \left\langle e^{i\mathbf{k}\mathbf{r}} \frac{\Psi(\mathbf{r}_1 + \mathbf{r}, \mathbf{r}_2, \ldots, \mathbf{r}_N)}{\Psi(\mathbf{r}_1, \mathbf{r}_2, \ldots, \mathbf{r}_N)} \right\rangle_{P(\mathbf{R},\mathbf{r})}. \quad (37)$$

To sample points $\mathbf{R} = (\mathbf{r}_1, \ldots, \mathbf{r}_N)$ in $2N$-dimensional configuration space, according to the density profiles $\rho(\mathbf{R}) = |\Psi(\mathbf{R})|^2$ of backflow wave functions for different particle numbers and parameters a and r_0 [see Eq. (25)], we use a standard Metropolis rejection algorithm,[39] which has the great advantage that it allows an arbitrarily complex distribution to be sampled in a straightforward way without knowledge of its normalization. For a very detailed description of the Metropolis algorithm but also for an overview on quantum Monte Carlo methods in general, we refer the reader to Ref. 40. Surely, the density profile $\rho(\mathbf{R})$ becomes very craggy as we approach the critical backflow strength $\alpha_c \approx 0.8$, where the zeros of the density form a scale-invariant fractal. Since the probability distribution of choice (36) does not depend on the coordinates $\mathbf{r}$, we just pick these points on the plane randomly.

The resulting normalized momentum distributions along the k_x direction for different values of α are shown in Fig. 5(a), where the error bars $\pm \sigma_f/\sqrt{n}$ are obtained from Eq. (35). We have used a relatively large small-distance cutoff $r_0 = 0.4 r_s$ to suppress the fractality of the nodal surfaces on smallest scales, leading to a highly oscillatory behavior of the integrands in the ultraviolet. For finite-size scaling, we have evaluated $n(k)$ for each value of α for various numbers of particles at a fixed density, leading to an increase in the momentum resolution, $\Delta k = 2\pi/L$. For different numbers of particles, we find a consistent interpolation of $n(\mathbf{k})$ for all values of α, indicating that the finite-size scaling is well behaved. In the inset of Fig. 5(a), the corresponding set of momenta entering the wave functions is shown. To avoid confusion, we would like to emphasize that these momentum states within the Fermi sphere are fully occupied only in the free fermion case. As seen in expansion (16) of the backflow wave functions in terms of free-particle states, backflow leads to a hierarchy of scattering processes, leading to a mixing of all kind of excited free-particle states and must therefore result in a drastic change in the quasiparticle momentum distribution.

For $\alpha = 0$ we obtain the discrete step function of the free Fermi gas. With increasing backflow strength α, the discontinuity Z decreases continuously, consistent with the picture that the bare particles get dressed with backflow clouds (see

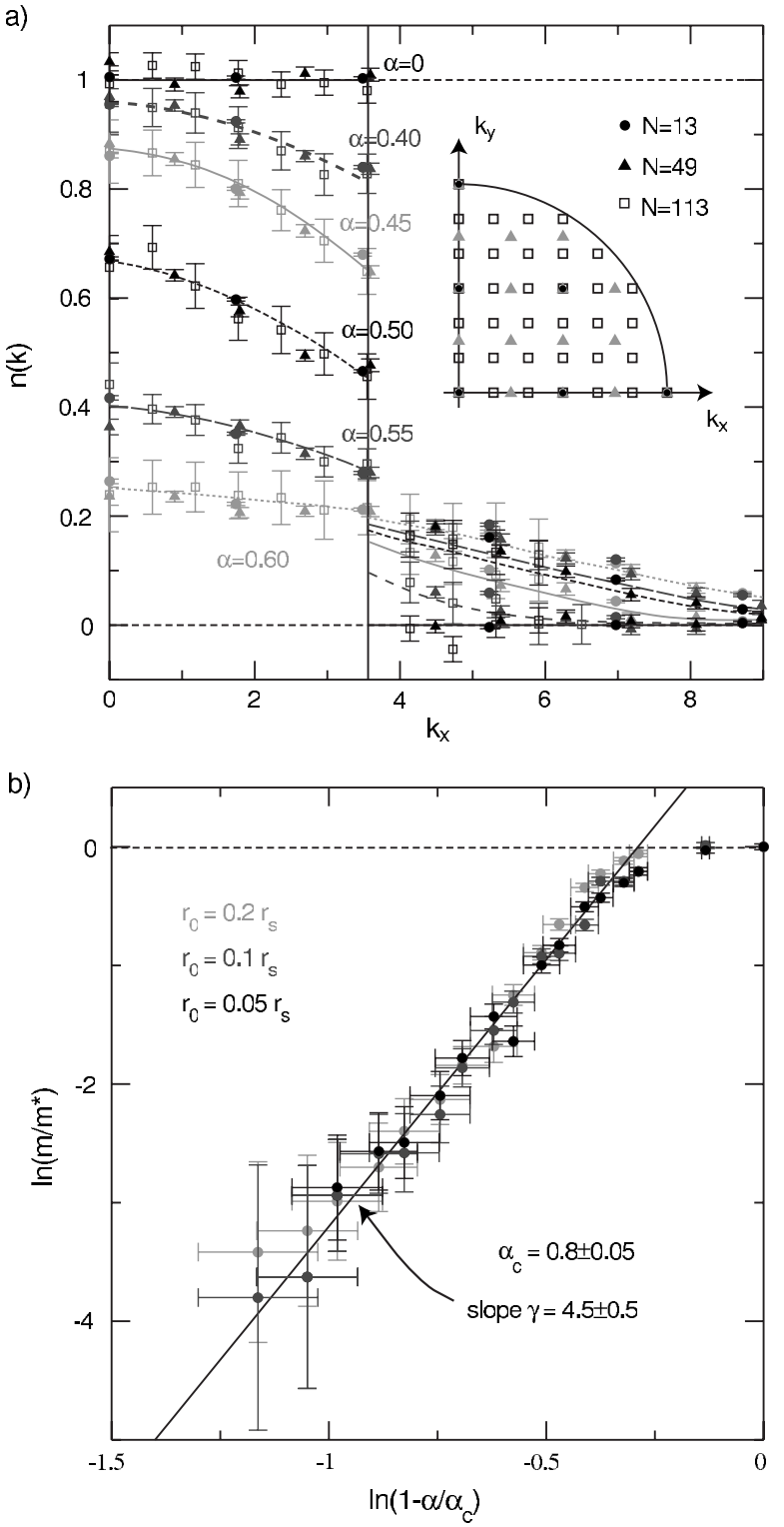

FIG. 5. (a) Momentum distribution $n(\mathbf{k})$ along k_x for different backflow strengths α for $N=13$ (filled circles), $N=49$ (filled triangles), and $N=113$ (open squares) particles at a fixed density. Here, a relatively large cutoff $r_0=0.4r_s$ has been used. (b) Inverse effective quasiparticle mass m/m^* as a function of α for $r_0/r_s=0.2,0.1,0.05$. m/m^* has been obtained from an interpolation of the discontinuity of $n(k)$. Due to numerical convergence problems, we were not able to follow the behavior for $\alpha>0.6$. Taking the value $\alpha_c \approx 0.8$ extracted from the correlation integral analysis, the behavior of $n(k)$ up to $\alpha=0.6$ suggests a strong mass divergence $m^*/m \sim (1-\alpha/\alpha_c)^{-\gamma}$ with $\gamma=4.5\pm0.5$.

Fig. 2), leading to an enhancement of the quasiparticle effective mass. In the regime of small backflow, we find the numerical convergence to be extremely fast, even for large systems. For larger values of α where the backflow clouds start to overlap (Fig. 2), Z starts to decrease very rapidly. Approaching the critical value $\alpha_c \approx 0.8$, where the nodal hypersurface turns into a fractal, for an increasing particle number N the signal-to-noise ratio goes down significantly. This critical slowing down in the numerics indicates that we are facing the singular limit of infinite number of particle correlations. For $\alpha>0.6$ it becomes impossible to extract the discontinuity since it becomes smaller than the numerical resolution. Qualitatively, a disappearance of the discontinuity at the critical value $\alpha_c \approx 0.8$, where the nodal surface turns into a fractal seems, consistent with the numerical data.

To extract the form of the effective-mass divergence $m^*/m \sim 1/Z$ as suggested by the disappearance of the discontinuity Z, we use the value $\alpha_c=0.8$ extracted from the corre-

lation integrals. We find that the behavior of $1/Z$ up to $\alpha=0.6$ is indeed consistent with a strong power-law divergence of the quasiparticle mass,

$$\frac{m^*}{m} \sim \left(1 - \frac{\alpha}{\alpha_c}\right)^{-\gamma}, \tag{38}$$

with an exponent $\gamma=4.5\pm0.5$ [see Fig. 5(b)]. Smaller values of the cutoff r_0 lead to a more rapid enhancement of the quasiparticle mass for very small values of α but do not influence the form of the effective-mass divergence. This indicates that the effective-mass divergence going hand in hand with the emergence of scale invariance of the nodal structure on large scales is driven by collective backflow correlations involving infinite particle interactions, or in diagrammatic language, infinite-order vertex "corrections."

VIII. CONCLUSION

In summary, employing the constrained path-integral formalism, we have delivered here proof of principle that fermion statistics and the emergent scale invariance underlying the critical state can be reconciled. We perceive it as highly profound that the workings of fermion statistics in interacting many-particle systems can be encoded in a geometrical structure (the nodal surface), which in turn can be married with the symmetry of scale invariance to yield a description of fermionic quantum critical states. Phenomenologically, the physics of fermion systems can be viewed as "boson dynamics times nodal-surface geometry;" at this level it is in principle a tractable problem to impose a fractal nodal surface, to subsequently compute propagators and thermodynamical properties. Of course, one anticipates that the fractal dimension of the nodal surface enters thermodynamic exponents and sets an anomalous dimension in the propagators. For the latter we have already found signatures from the diffusive behavior imposed by the fractal nodal surface generated by backflow. Instead of conventional Gaussian diffusion, we find superdiffusive behavior corresponding to single-particle propagators acquiring a Levy-flight form. In principle, there is hope for a generalization of Kadanoff-type scaling relations or of Wilsonian renormalization-group treatment of fermionic systems around such non-Gaussian quantum critical points.

Also, the competition with superconductivity can be studied: it has been demonstrated that the nodal structure associated with BCS superconductors is subtly different from that of Fermi gases,[41] and it would be quite interesting to find out how this affair would work out starting from a fermionic critical state. Naively, one expects that a fractal nodal surface imposing constraints on the dynamics on all length and time scales would lead to a drastic enhancement of pairing, which might be the reason why quite generically instabilities toward superconducting order in the vicinity of fermionic quantum critical points have been observed.

We have used here the backflow wave function just as a device to generate a fractal nodal surface, leaving open what the actual microscopic conditions are, causing criticality in the physical systems. Backflow is associated with the effective incompressible nature of the fluid flow and this has an interesting resemblance to the microscopy of the strongly correlated electron systems: in one or the other way, the Mott insulator is close by when fermionic quantum criticality is observed and "Mottness" renders electron systems incompressible. In fact, the physics associated with backflow is quite similar to the interpretation given by Anderson[42] of the "strange metal" as a Gutzwiller-projected fermion system, in the sense that both approaches are based on a hidden quasiparticle picture and involve singular transformations of the Fermi liquid state. Further investigation is needed as to what sense the nodal structures associated with Gutzwiller-projected wave functions are scale invariant and resemble critical states of fermionic matter.

Very recently, Senthil[43] formulated scaling hypotheses for fermionic critical points by assuming that although the Landau quasiparticles cease to exist at the critical point, there might still be a sense of an underlying critical Fermi surface characterized by a higher-order kink singularity rather than a jump in the momentum distribution.[43,44] In the case of the critical backflow state, we cannot rule out such a possibility and further investigation is required as to whether the nonlocal nature of the nodal constraint structure, which has to be responsible for the formation of a sharp Fermi surface in a Fermi liquid at zero temperature,[22] might lead to residual critical Fermi-surface structures in the critical regime.

ACKNOWLEDGMENTS

We acknowledge insightful discussions with S. C. Zhang, A. V. Balatsky, L. Mitas, and D. M. Ceperley. This research was supported by the Nederlandse Organisatie voor Wetenschappelijk Onderzoek (NWO) and by the Stichting voor Fundamenteel Onderzoek der Materie (FOM).

APPENDIX: NODE SEARCHING

To find the nodes of the free fermion and Feynman backflow wave functions, we have to track the sign changes of $\Psi(\mathbf{R})$ on a numerical grid where the nodal structure has to look smooth on the scale of the grid size ϵ. Obviously, it is not possible to map out the full high-dimensional nodal hypersurface in dN-dimensional configuration space. Instead, we calculate the nodal structures on random two-dimensional cuts, obtained by keeping $N-1$ particles fixed at random positions $\mathbf{r}_2,\ldots,\mathbf{r}_N$, and tracking down the zeros of the wave function when moving the remaining particle $\mathbf{r}_1$ over the system $[-L/2,L/2]\times[-L/2,L/2]$,

$$\Omega_{\mathbf{r}_2,\ldots,\mathbf{r}_N} = \{\mathbf{r}_1 | \Psi(\mathbf{r}_1,\mathbf{r}_2,\ldots,\mathbf{r}_N) = 0\}. \tag{A1}$$

If the nodal surface is not fractal, this defines a one-dimensional hypersurface in the $(d=2)$-dimensional configuration space of the particle $\mathbf{r}_1$. To calculate the values of backflow wave functions on a certain grid point, we have to evaluate an $(N\times N)$-dimensional determinant, $\det \mathbf{A}$, with $a_{ij}=\exp(i\mathbf{k}_i\tilde{\mathbf{r}}_j)$ and with the collective backflow coordinates given in Eq. (14). This is done by factoring into lower and upper triangular matrices for inversion using $\mathbf{A}=\mathbf{LU}$, where $\mathbf{L}$ and $\mathbf{U}$ are lower and upper triangular matrices of dimension $N\times N$, respectively. This decomposition is unique if we

require $l_{ii}=1$ for the diagonal elements of $\mathbf{L}$. In this case, the determinant is given by

$$\det \mathbf{A} = \det(\mathbf{L}\cdot\mathbf{U}) = \det(\mathbf{L})\det(\mathbf{U}) = \prod_{i=1,\ldots,N} u_{ii}. \quad \text{(A2)}$$

It is easy to check that one can adjust the overall prefactor of the wave function to make it real valued. This is a necessary condition to obtain the nodes by the sign changes of Ψ.

It becomes immediately clear why the collective backflow makes it is much harder to calculate the nodes. In the case of free fermions ($\alpha=0$), we have $\tilde{\mathbf{r}}_i=\mathbf{r}_i$ and by moving the particle $\mathbf{r}_1$ over the cut, we change only the first row of the matrix $\mathbf{A}$. Therefore we can use the expansion

$$\det(\mathbf{A}) = \sum_{i=1,\ldots,N} (-1)^{1+i} a_{1i} \det(\mathbf{A}_{1i}), \quad \text{(A3)}$$

where $\mathbf{A}_{1i}$ denotes the $(N-1)\times(N-1)$ matrix obtained by dropping the first row and the ith column of the matrix $\mathbf{A}$. Only the prefactors a_{1i} depend on the coordinate $\mathbf{r}_1$, whereas the subdeterminants have to be calculated only once for a particular cut. Including backflow, the change in the position $\mathbf{r}_1$ of the first particle leads to a change in all collective coordinates $\{\tilde{\mathbf{r}}_i\}$ at the same time and the above expansion turns out to be useless. Instead, on every grid point we have to recalculate all collective coordinates and the full $N\times N$ determinant.

To track the sign changes on the cut, we use two different algorithms. The first one is based on a triangulation in the vicinity of the nodal lines (see Fig. 6) avoiding the calculation of the wave function on too many points away from the nodes. A first point on the node is found by following a random walk until we encounter a sign change, say, between points A_1 and B_1. We now initialize our triangulation procedure by choosing one of the two possibilities of completing side A_1B_1 to an equilateral triangle $\Delta_1=A_1B_1C_1$. If the nodal structure is smooth on the scale ϵ of the numerical grid, the nodal line has left the triangle through one of the two new sides B_1C_1 or A_1C_1; in our example it crosses the side B_1C_1 since $\Psi(B_1)\Psi(C_1)<0$, whereas $\Psi(A_1)\Psi(C_1)>0$. We now take the mirror image A_2 of point A_1 with respect to side B_1C_1 to obtain the next triangle $\Delta_2=B_1C_1A_2$ and repeat the procedure. Using this triangulation, we directly follow the nodal line.

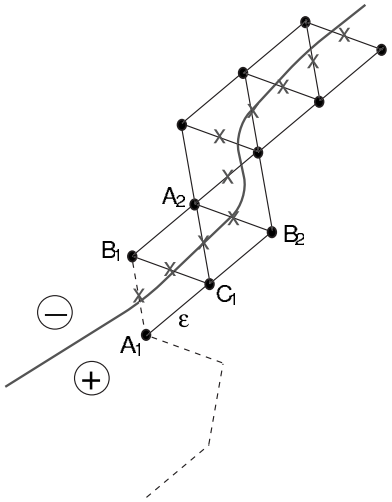

FIG. 6. Illustration of the algorithm following a nodal line by a triangulation method.

Obviously, the above procedure breaks down when a triangle is penetrated by two nodal lines or when a line leaves the triangle through the same side it had entered. Therefore, the grid size ϵ has to be sufficiently small. In particular, even for small backflow, the nodal surfaces develop a local fractality (see Fig. 3) which is suppressed on smallest scales by the UV cutoff r_0. Hence we have to fulfill the requirement $\epsilon \ll r_0$ so as to not run into problems.

For illustrational purposes, it is desirable to calculate the wave function on all points of a two-dimensional $n\times n$ grid where $\epsilon=L/n$. This method has been used for Fig. 2, where the nodal lines correspond to the interface between positive (red) and negative (blue) regions. The absolute values of Ψ are encoded in the color shading.

[1] A. J. Schofield, Contemp. Phys. **40**, 95 (1999).
[2] P. Coleman, C. Pépin, Q. Si, and R. Ramazashvili, J. Phys.: Condens. Matter **13**, R723 (2001).
[3] Q. Si, S. Rabello, K. Ingersent, and J. L. Smith, Nature (London) **413**, 804 (2001).
[4] G. R. Stewart, Rev. Mod. Phys. **73**, 797 (2001).
[5] J. Custers, P. Gegenwart, H. Wilhelm, Y. Tokiwa, O. Trovarelli, C. Geibel, F. Steglich, C. Pépin, and P. Coleman, Nature (London) **424**, 524 (2003).
[6] S. Paschen, T. Lühmann, S. Wirth, P. Gegenwart, O. Trovarellii, C. Geibel, F. Steglich, P. Coleman, and Q. Si, Nature (London) **432**, 881 (2004).
[7] H. Takagi, B. Batlogg, H. L. Kao, J. Kwo, R. J. Cava, J. J. Krajewski, and W. F. Peck, Phys. Rev. Lett. **69**, 2975 (1992).
[8] S. Sachdev, *Quantum Phase Transitions* (Cambridge University Press, Cambridge, England, 1999).
[9] D. van der Marel, H. J. A. Molegraaf, J. Zaanen, Z. Nussinov, F. Carbone, A. Damascelli, H. Eisaki, M. Greven, P. H. Kes, and M. Li, Nature (London) **425**, 271 (2003).
[10] J. Orenstein and A. J. Millis, Science **288**, 468 (2000).
[11] L. J. Zhu, M. Garst, A. Rosch, and Q. Si, Phys. Rev. Lett. **91**, 066404 (2003).
[12] J. Zaanen and B. Hosseinkhani, Phys. Rev. B **70**, 060509(R) (2004).
[13] J. Zaanen, Nature (London) **430**, 512 (2004).
[14] C. M. Varma, Phys. Rev. B **55**, 14554 (1997).
[15] J. Zaanen, Science **319**, 1205 (2008).
[16] M. Troyer and U. J. Wiese, Phys. Rev. Lett. **94**, 170201 (2005).
[17] D. M. Ceperley, J. Stat. Phys. **63**, 1237 (1991).
[18] R. P. Feynman and M. Cohen, Phys. Rev. **102**, 1189 (1956).
[19] D. M. Ceperley, Phys. Rev. Lett. **69**, 331 (1992).
[20] C. Pierleoni, D. M. Ceperley, B. Bernu, and W. R. Magro, Phys.

Rev. Lett. **73**, 2145 (1994).
[21] W. R. Magro, D. M. Ceperley, C. Pierleoni, and B. Bernu, Phys. Rev. Lett. **76**, 1240 (1996).
[22] J. Zaanen, F. Krüger, J.-H. She, D. Sadri, and S. I. Mukhin, arXiv:0802.2455 (unpublished).
[23] T. Giamarchi, *Quantum Physics in One Dimension* (Oxford Science, New York, 2004).
[24] V. L. Pokrovsky and A. L. Talapov, Phys. Rev. Lett. **42**, 65 (1979).
[25] J. Zaanen, Phys. Rev. Lett. **84**, 753 (2000).
[26] S. I. Mukhin, W. van Saarloos, and J. Zaanen, Phys. Rev. B **64**, 115105 (2001).
[27] W. Helfrich, Z. Naturforsch. A **33**, 305 (1978).
[28] L. Mitas, Phys. Rev. Lett. **96**, 240402 (2006).
[29] L. Mitas, arXiv:cond-mat/0605550 (unpublished).
[30] K. E. Schmidt, M. A. Lee, M. H. Kalos, and G. V. Chester, Phys. Rev. Lett. **47**, 807 (1981).
[31] Y. Kwon, D. M. Ceperley, and R. M. Martin, Phys. Rev. B **48**, 12037 (1993).
[32] M. Holzmann, D. M. Ceperley, C. Pierleoni, and K. Esler, Phys. Rev. E **68**, 046707 (2003).
[33] A. C. Calder, M. R. Curry, R. M. Panoff, and Y. J. Wong, Phys. Rev. E **53**, 5450 (1996).
[34] J. Casulleras and J. Boronat, Phys. Rev. Lett. **84**, 3121 (2000).
[35] P. Grassberger and I. Procaccia, Phys. Rev. Lett. **50**, 346 (1983).
[36] F. Dyson, Phys. Rev. **75**, 1736 (1949).
[37] A. A. Abrikosov, L. P. Gorkov, and I. E. Dzyaloshinski, *Methods of Quantum Field Theory in Statistical Physics* (Dover, New York, 1975).
[38] W. Feller, *An Introduction to Probability Theory and Its Applications* (Wiley, New York, 1968).
[39] N. Metropolis, A. W. Rosenbluth, M. N. Rosenbluth, A. H. Teller, and E. Teller, J. Chem. Phys. **21**, 1087 (1953).
[40] W. M. C. Foulkes, L. Mitas, R. J. Needs, and G. Rajagopal, Rev. Mod. Phys. **73**, 33 (2001).
[41] V. K. Akkineni, D. M. Ceperley, and N. Trivedi, Phys. Rev. B **76**, 165116 (2007).
[42] P. W. Anderson, Nat. Phys. **2**, 626 (2006).
[43] T. Senthil, the preceding paper, Phys. Rev. B **78**, 035153 (2008).
[44] T. Senthil, Ann. Phys. **321**, 1669 (2006).